Resilience Enhancement of Electric Power Distribution Grids against Wildfires

Mostafa Nazemi, *Student Member, IEEE*, Payman Dehghanian, *Senior Member, IEEE*, Mohannad Alhazmi, *Student Member, IEEE*, and Yousef Darestani

2021 IEEE Industry Applications Society Annual Meeting (IAS) | 978-1-7281-6401-4/21/$31.00 ©2021 IEEE | DOI: 10.1109/IAS48185.2021.9677372

***Abstract*—Wildfires have been growingly recognized as a prominent threat in regions with high temperatures during the summer. Power distribution systems, especially those passing through forest regions, are exposed and highly vulnerable to wildfires. This paper applies a general formulation to enhance the operational resilience of power distribution networks equipped with renewable energy resources (RESs), e.g., wind and solar energy, micro turbines (MTs) as well as energy storage systems (ESSs) when exposed to progressive wildfires. The wildfire event is characterized comprehensively and the dynamic line rating (DLR) of overhead distribution branches is used to model the impacts of wildfires on distribution power lines. A scenario-based optimization formulation is applied to tackle the system prevailing uncertainties. The applied framework is evaluated on the IEEE 33-node test system and the numerical results reveal the promising efficacy of the methodology.**

***Index Terms*—Power distribution systems; wildfire hazards; distributed energy resources; resilience.**

NOMENCLATURE

A. Abbreviations

DLR	Dynamic line rating
ESSs	Energy storage systems
RESs	Renewable energy resources
MTs	Micro-turbines
PV	Photovoltaic energy
WT	Wind turbine
SoC	State of charge

B. Sets and Indices

$i, j \in \mathbf{N_B}$	Indices/set of nodes.
$ij \in \mathbf{L}$	Indices/set of distribution lines between nodes i and j.
$t \in \mathbf{N_T}$	Indices/set of time periods.
$N_\mathbf{B}, N_\mathbf{T}, N_\mathbf{L}$	Number of all nodes, time periods, and branches.
$\omega \in \Omega$	Index/set of scenarios.
S	Set of all PV panels.

C. Parameters and Constants

1) Fire Parameters:

T^f	Flame zone temperature ($^\circ k$).
ν^f	Fire front length (m).
α^f	Fire tilt angle (rad).
ρ^b	The bulk density of the fuel (kg/m^3).
ε^f	Flame zone emissivity.

2) Environmental Conditions:

τ	Dimensionless atmospheric transmissivity.
B	Stefan-Boltzman constant (W/m^2K^4).
V^{wind}	Wind speed (m/s).
σ^{wind}	Angle between the fire and power line conductors (rad).
T^a	Ambient temperature ($^\circ k$).
k^a	Thermal conductivity of air (W/mK).
μ^α	Air dynamic viscosity (kg/ms).
ρ^α	Air density (kg/m^3).
K^0	Shape index of the Weibull distribution.
C	Scale index of the Weibull distribution.

3) Conductor Specifications:

mC_p	Total heat capacity of conductor (J/mK).
D	Conductor diameter (m).
K	Solar absorptivity.
ϕ^{sun}	Solar radiation rate (W/m^2).
$R_{ij,a}$	Ambient line resistance.
$T^{\max}$	Maximum permitted conductor temperature ($^\circ k$).

4) Price and Costs:

VoLL	Value of lost load ($/MWh).
c^D	Selling electricity price ($/MWh).
c^{MT}	MTs generation cost ($/MW).
$c^{su/sd}$	MTs switching cost ($).

5) Power Distribution System Components:

$P^{\text{demand}}_{i,\omega,t}$	Real power demand at node i at time t (MW).
$Q^{\text{demand}}_{i,\omega,t}$	Reactive power demand at node i at time t (MVar).
n^{ST}	Conversion efficiency of ESSs.
E^{ST}	Energy capacity of ESSs (MWh).

D. Functions and Variables

1) Fire Model:

$\theta^f_{ij,t}$	View angle between fire and conductor line ij at time t (rad).
$d^f_{ij,t}$	Distance between fire and line ij at time t (m).
V^f_t	Fire spread rate (m/s) at time t.
$T_{ij,t}$	Conductor temperature of line ij at time t ($^\circ k$).
χ^f_t	Radiative heat flux at time t (W/m^2).

This work was supported in part by the National Science Foundation (NSF) under Grant ICER-2022505. M. Nazemi, P. Dehghanian, and M. Alhazmi are with the Department of Electrical and Computer Engineering, George Washington University, Washington, DC 20052, USA.

Y. Darestani is with the Department of Civil and Environmental Engineering, Michigan Technological University, Houghton, MI 49931, USA.

2) Heat Gain and Loss:

$q_{ij,t}^{\text{line}}$	Resistance heat gain rate of line ij at time t (W/m).
$q_{ij,t}^{\text{sun}}$	Solar heat gain rate of line ij at time t (W/m).
$q_{ij,t}^{\text{fire}}$	Fire heat gain rate of line ij at time t (W/m).
$q_{ij,t}^{\text{con}}$	Convection heat loss rate of line ij at time t (W/m).
$q_{ij,t}^{\text{rad}})$	Radiation heat loss rate of line ij at time t (W/m).

3) Power System Model:

$p_{i,t}^{D}, q_{i,t}^{D}$	Real and reactive power supplied at node i at time t (MW, MVar).
$P_{ij,t}^{\text{fl}}, Q_{ij,t}^{\text{fl}}$	Real and reactive power flow on branch ij at time t (MW, MVar).
$\text{SoC}_{i,t}^{ST}$	SoC of ESS at time t.
$p_{i,\omega,t}^{\text{Ch}}, p_{i,\omega,t}^{\text{DC}}$	Charging and discharging power of ESS at node i at time t (MW).
$p_{i,t}^{\text{MT}}, q_{i,t}^{\text{MT}}$	Real and reactive power output of MT at node i (MW, MVar).
$P_{i,t}^{\text{WT}}, P_{i,t}^{S}$	Real power output of WT and PV at node i at time t (MW).
$V_{\text{sqr}_{i,t}}$	Squared voltage magnitude at node i at time t (kV^2).
$p_{i,t}^{\text{shed}}, q_{i,t}^{\text{shed}}$	Real and reactive load shedding at node i at time t (MW, MVar).
p_{t}^{UP}	Active power exchange with the upstream network at time t (MW).

E. Binary Variables

$\alpha_{ij,t}$	Connection status of branch ij at time t (1 if the branch is connected, 0 otherwise).
$u_{i,t}^{\text{SoC}}$	Charging and discharging status of ESS at node i at time t (1 if charging, 0 otherwise).
$u_{i,t}$	Status of MT at node i at time t (1 if the MT is generating, 0 otherwise).
φ_{t}^{UP}	Buying or selling energy from/to the up stream network at time t (1 if buying, 0 otherwise).

I. Introduction

THE growing severity and duration of power outages triggered by wildfires impose an adverse impact on the operation of multiple life-line networks and results in significant financial risks. For instance, in May 2016, a wildfire was initiated in Alberta, Canada. The direct financial loss to insurance providers from the great Alberta fire was estimated at about $3.7 billion [1]. In October 2017, a series of wildfires started to burn across the wine county of Northern California. These wildfires caused at least $9.4 billion in insured damages and the death of 44 people [2]. In fiscal year 2017, the cost of battling blazes topped $2.4 billion [3]. For the first time in its 110-year history, the U.S. Forest Service is spending more than 50 percent of its budget fighting wildfires [4]. The California Department of Forestry and Fire Protection reports that the 2018 Woolsey and Camp fires caused $4 billion and $11 billion in damages, respectively [5]. In addition, wildfire risks in October 2018 and 2019 forced Pacific Gas and Electric to anticipatively cut off electricity to a sizable number of end-use consumers in high-risk areas in northern California, resulting in missed opportunity costs though no wildfires happened [6]. Therefore, one can notice that maintaining the nation's electric power system resilience against wildfires and ensuring a reliable, secure, and sustainable supply of electricity during such threatening events are among the top priorities for the electric power industry.

Several papers in the literature have studied the power system's resistance to severe fire conditions. Among which, the thermal rating of the at-risk power lines was dynamically adjusted in [7] to reduce the line heat gained from the fire. In order to model the effect of wildfires on conductor temperature and consequently on the flowing current, reference [8] suggested a DLR mechanism for overhead lines. Reference [9] proposed a technique for quantifying the destruction caused by wildfires to electric distribution grids. In [10], [11], a strategy for optimal distribution system operation in the face of a huge fire is introduced, where the operating performance of microgrids and the role of demand response programs are investigated. Reference [12] examines different faults and situations that contribute to wildfire ignition, establishing the mathematical relation between the wind speed and fire ignition risk. A statistical characterization model is developed in [13] to demonstrate the relationship between continuous ignition of a dry fuel bed and multiple determining parameters such as wind speed, fuel moisture content, and arc length. While the models in [11]–[14] are important to understand the wildfire ignition problem, the literature lacks a comprehensive model that characterizes wildfire propagation and its impacts on overhead line's temperature in power distribution systems.

The wildfire impacts on power transmission and distribution lines are not limited to the actual destruction of the structures. In case of a major wildfire, such as one in a forest, the wooden poles would most likely catch fire and the conductors would melt. However, there are many small or moderate wildfires with a long front length in areas with low-height combustibles that pose thermal stress on overhead wires where even if there is no physical damage to the system, the flame and smoke may have an indirect effect on the line's transmitting capability [15]. Furthermore, an increase in the conductor's surface temperature will influence the conductor's rate of annealing and decrease its tensile strength. Therefore, it is vital to develop a comprehensive methodology to study the dynamic operation of microgrids in face of massive wildfires. This paper focuses on the resilient operation of power distribution systems exposed to an approaching wildfire where a DLR model is developed based on [8] to capture the impacts of wildfire on the conductor's temperature.

The rest of the paper is organized as follows. Section II introduces a general wildfire model while the problem formulation is provided in Section III. Numerical case study and simulation results on a modified IEEE 33-bus test system are demonstrated in Section IV. The paper is eventually concluded in Section V.

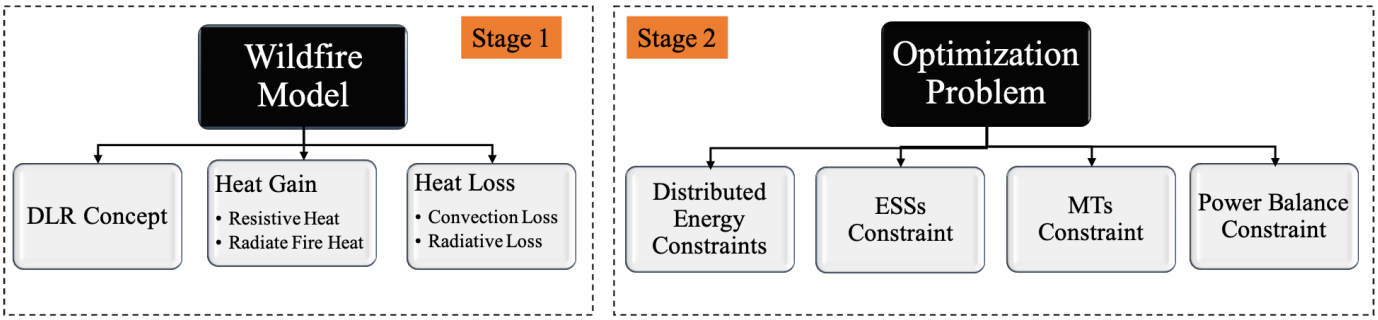

Fig. 1. The big-picture architecture of the problem.

II. Wildfire Modeling Formulation

The big picture of the applied framework is shown in Fig. 1. The applied framework consists of two stages. In the first stage, the progressive wildfire is modeled based on the DLR concept [8] where the dynamic temperature of conductors is determined per the heat gain and loss in different time periods. In stage 2, the optimization problem formulation is applied where different types of constraints related to power system operation and fire behavior are included, linearized, and then convexified to be solved by off-the-shelf optimization solvers. The details of each stage are presented in the following.

A. Wildfire Model

The applied wildfire model used in this paper is comprehensively introduced for the first time in [8]. Wildfire heat is transferred through radiation and convection. Convective transmission is not of concern in this paper since it influences the temperature of the conductors only when the fire is exactly under the overhead line. The radiative heat flux χ^f from the entire flame transmitted to a conductor is then calculated using the geometry of the flame and the fire front properties as follows:

$$\chi^f_{ij,\omega,t} = \frac{\tau \cdot \varepsilon^f \cdot B \cdot {T^f}^4}{2} \cdot \sin(\theta^f_{ij,\omega,t}) \tag{1}$$

where τ, ε^f and B are all parameters related to the environment. T^f is the temperature of the fire front set as $1200°k$ [16], and θ^f is the view angle between the threatened line and the fire front expressed in the following:

$$\theta^f_{ij,\omega,t} = \tan^{-1}\left(\frac{\nu^f \cdot \cos(\alpha^f)}{d^f_{ij,\omega,t} - (\nu^f \cdot \sin(\alpha^f))}\right) \tag{2}$$

where ν^f represents the length of the fire and d^f indicates the distance between wildfire and the affected conductor which is computed in (3).

$$d^f_{ij,\omega,t} = d^f_{ij,\omega,t-1} \cdot V^f_{\omega,t} \cdot \Delta t \cdot \cos(\sigma^{\text{wind}}_{ij,\omega,t}) \tag{3}$$

$$V^f_{\omega,t} = \frac{k \cdot (1 + V^{\text{wind}}_{\omega,t})}{\rho^b} \tag{4}$$

V^f (m/s) is the specific rate of flame spread in wildland on a flat ground that depends on the wind speed V^{wind}(m/s). ρ^b is the bulk density of the fuel equal to 40 kg/m^3 in the forest. k is equal to 0.07 for wildland fire and 0.05 for wood crib [7].

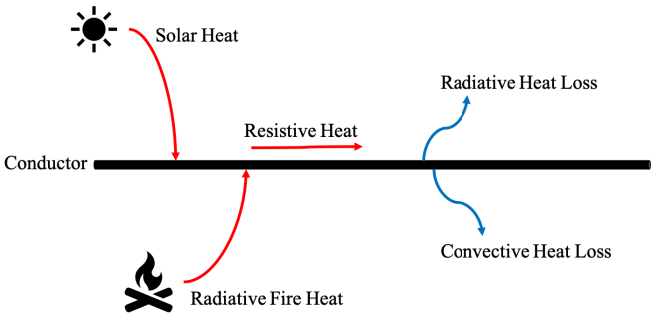

Fig. 2. Illustration of different types of heat gain and heat loss for a conductor in the event of wildfire.

B. On the Concept of DLR

According to [8], the power line conductor's total heat is the multiplication of coefficients and heat loss rates— i.e., the convective heat loss rate q^{con}, the radiative heat loss rate q^{rad}—, as well as heat gain rates—i.e., ohmic losses resistance of the power line q^{line}, radiative heat flux from fire q^{fire} and solar heat gain rate q^{sun}. Figure 2 illustrates different types of heat gain and loss for a power line conductor. Therefore, any changes in the temperature at any time interval is calculated using the following non-steady-state heat equation which is a first-order nonlinear differential constraint:

$$\begin{aligned}(T_{ij,\omega,t+1} - T_{ij,\omega,t}) = \frac{\Delta t}{mC_p} \cdot (q^{\text{line}}_{ij,\omega,t} + q^{\text{sun}}_{ij,\omega,t} + q^{\text{fire}}_{ij,\omega,t} \\ - q^{\text{con}}_{ij,\omega,t} - q^{\text{rad}}_{ij,\omega,t})\end{aligned} \tag{5}$$

Each of the above terms are explained as follows.

1) Heat Gain: In the given equation, the heating terms are the solar heat energy that the conductor can absorb, the resistive thermal energy produced by currents flowing through the power line conductor, and the fire radiation heat measured as follows:

$$q^{\text{sun}}_{ij,\omega,t} = D_{ij} \cdot K_{ij} \cdot \phi^{\text{sun}}_{ij,\omega,t} \tag{6}$$

$$q^{\text{line}}_{ij,\omega,t} = R^{\text{line}}(T_{ij,\omega,t}) \cdot (I_{ij,\omega,t})^2 \tag{7}$$

$$q^{\text{fire}}_{ij,\omega,t} = D_{ij} \cdot \chi^{\text{f}}_{ij,\omega,t} \tag{8}$$

In equation (6), D_{ij} is the diameter of the conductors and $\phi^{\text{sun}}_{ij,\omega,t}$ is the sun radiation rate. K_{ij} is the solar absorptivity that varies between 0.27 for the bright stranded aluminum conductor and 0.95 for the weathered conductor in an industrial environment. A value of 0.5 is often used if nothing is

known about the conductor absorptivity [17]. In equation (7), $R^{\text{line}}(T_{ij,\omega,t})$ reflects a function that describes the relationship between the resistance of the power line conductor and its temperature. $R_{ij,a}$ is the resistance of the line at ambient temperature $T_{ij,a}$ ($298°k$). d_{ij} is the conductor thermal resistant coefficient.

$$R^{\text{line}}(T_{ij,\omega,t}) = R_{ij,a} \cdot (1 + d_{ij} \cdot (T_{ij,\omega,t} - T_{ij,a})) \quad (9)$$

2) Heat Loss: The last two terms in (5) account for the cooling down of the power line conductor. The convection loss in this paper is considered as the conductor is cooled down via a cylinder of moving air around the conductor. The convection heat loss is the largest value between high-speed wind $q^{\text{con}}_{ij,\omega,t,(\text{high})}$ and low-speed wind $q^{\text{con}}_{ij,\omega,t,(\text{low})}$ according to the IEEE standard [18]. Equations (10) and (11) represent the calculation of the convection loss.

$$q^{\text{con}}_{ij,\omega,t,(\text{high})} = K_{\text{angle}} \cdot 0.754 \cdot N_{Re}^{0.6} \cdot k^a \cdot (T - T^a) \quad (10)$$

$$q^{\text{con}}_{ij,\omega,t,(\text{low})} = K_{\text{angle}} \cdot [1.01 + 1.35 \cdot N_{Re}^{0.52}] \cdot k^a \cdot (T - T^a) \quad (11)$$

The magnitude of the equation depends on N_{Re}, the Reynolds number and wind direction factor K_{angle} given by:

$$N_{Re} = \frac{D_{ij} \cdot \rho^{\alpha} \cdot V^{\text{wind}}_{\omega,t}}{\mu^{\alpha}} \quad (12)$$

$$K_{\text{angle}} = 1.194 - \cos(\sigma^{\text{wind}}_{ij,\omega,t}) + 0.194\cos(2\sigma^{\text{wind}}_{ij,\omega,t}) + 0.368\sin(2\sigma^{\text{wind}}_{ij,\omega,t}) \quad (13)$$

Next, the cable radiated heat rate can be described by the following equation:

$$q^{\text{rad}}_{ij,\omega,t} = 17.8 D^{ij} \cdot \epsilon \cdot [(\frac{T_{ij,\omega,t}}{100})^4 - (\frac{T_{ij,a}}{100})^4] \quad (14)$$

More detailed information is available in [8], [19].

III. Problem Formulation

A. Optimization Problem Formulation

Based on [8], [19], a linear optimization model is used to boost the power distribution system resilience in the face of progressive wildfires. Although resilience is directly linked to load outages [20], operating costs should also be considered to ensure the most cost-effective solution during the emergency operating conditions when facing a progressive wildfire. Therefore, the objective function is designed to minimize the expected cost as expressed below:

$$\begin{aligned}\min(&\sum_{t=1}^{N_T}\sum_{\omega=1}^{N_\Omega}\pi_\omega \cdot \sum_{i=1}^{N_B}(\text{VoLL} \cdot p^{\text{shed}}_{i,\omega,t} - c^D \cdot p^D_{i,\omega,t}) \\ &+ \sum_{t=1}^{N_T}\sum_{\omega=1}^{N_\Omega}\pi_\omega \cdot \sum_{i=1}^{N_B}(c^{\text{MT}} \cdot p^{\text{MT}}_{i,\omega,t}) + \sum_{t=1}^{N_T}\sum_{i=1}^{N_B}(su^{\text{MT}}_{i,t} + sd^{\text{MT}}_{i,t})) \\ &+ \sum_{t=1}^{N_T}\sum_{\omega=1}^{N_\Omega}\pi_\omega \cdot c^{\text{UP}}_t \cdot (p^{\text{UP}_B}_{\omega,t} - p^{\text{UP}_S}_{\omega,t})\end{aligned} \quad (15)$$

In the first line, $\text{VoLL} \cdot p_{i,\omega,t}$ represents the load shedding cost and $c^D \cdot p^D_{i,\omega,t}$ indicates the revenue from providing energy to the end customers. The second and third terms represent the generation, start-up, and shut down costs of MTs. The last term represents the power exchange cost with the upstream network. To optimally operate the power distribution network during a progressive wildfire event, multiple constraints should be considered as described in the following.

1) Distributed Energy Constraints: RESs, i.e., wind and solar energy, is considered in this paper that can be utilized when the fire hits the power distribution grid. To tackle the uncertain nature of RESs, the Weibull and von Mises distributions are considered. Suppose that the wind speed V^{wind} is a stochastic quantity with the following probability density function:

$$f(V^{\text{wind}}) = \frac{K^0}{C^k} \cdot V^{K^0-1} \cdot e^{(-V/C)^{K^0}} \quad (16)$$

where K^0 and C are the shape index and the scale index of the Weibull distribution. In this paper, a k-factor of 2 and standard deviation equal to 15% of the mean value are considered for wind speed and direction as well as solar illumination which can be used as inputs to the optimization engine. The relationship between the output power of a wind generating unit and the wind speed can be formulated as follows:

$$\begin{aligned} P^{\text{WT}}_{i,t} &= 0, \quad 0 \le v \le v_{ci} \quad \text{or} \quad v_{co} \le v \\ P^{\text{WT}}_{i,t} &= P^w_{\text{rated}} \cdot (\frac{v - v_{ci}}{v_r - v_{ci}}), \quad v_{ci} \le v \le v_r \\ P^{\text{WT}}_{i,t} &= P^w_{\text{rated}}, \quad v_r \le v \le v_{co} \end{aligned} \quad (17)$$

Where v is the wind speed at the hub height of the wind unit; v_{ci}, v_{co}, and v_r are, respectively, the cut-in wind speed, the cut-out wind speed, and the rated wind speed; and P^w_{rated} is the rated output power of the wind unit [21].

As for the solar power, the illumination intensity is usually considered the dominant factor affecting the output power of the solar panel. The relationship between the illumination intensity and the output power of a solar generating unit can be described as follows:

$$\begin{aligned} P^S_{i,t} &= P^S_{\text{rated}} \cdot (\frac{S}{S_r}), \quad 0 \le S \le S_r \\ P^S_{i,t} &= P^S_{\text{rated}}, \quad S_r \le S \end{aligned} \quad (18)$$

Where S is the illumination intensity, S_r is the rated value, and P^S_{rated} indicates the rated output power of the solar cells.

2) MTs Constraints: The active and reactive output power of MTs and their start-up and shut-down costs have to be considered as follows to guarantee the power balance in the system at the minimum cost.

$$p^{\text{MT}}_{i(\min)} \cdot u^{\text{MT}}_{i,t} \le p^{\text{MT}}_{i,\omega,t} \le p^{\text{MT}}_{i(\max)} \cdot u^{\text{MT}}_{i,t} \quad (19)$$

$$q^{\text{MT}}_{i(\min)} \cdot u^{\text{MT}}_{i,t} \le q^{\text{MT}}_{i,\omega,t} \le q^{\text{MT}}_{i(\max)} \cdot u^{\text{MT}}_{i,t} \quad (20)$$

$$sd^{\text{MT}}_{i,t} \ge c^{SD}_i \cdot (u^{\text{MT}}_{i,t} - u^{\text{MT}}_{i,t-1}) \ge 0 \quad (21)$$

$$su^{\text{MT}}_{i,t} \ge c^{SU}_i \cdot (u^{\text{MT}}_{i,t} - u^{\text{MT}}_{i,t-1}) \ge 0 \quad (22)$$

where (19) and (20) determine the maximum and minimum limits for active and reactive power of MTs, respectively; equations (21) and (22) reflect the start up and shut down costs of the turbines, respectively. The binary variable $u_{i,t}$ is

used to determine the status of MTs, i.e., 1 for start up and 0 for shut down and the corresponding costs c_i^{SD} and c_i^{SU} are considered the same.

3) ESSs Constraints: The operation constraints of ESSs can be expressed as follows.

$$\mathrm{SoC}_{i,\omega,t}^{ST} = \mathrm{SoC}_{i,\omega,t-1}^{ST} + (\frac{n_i^{ST} \cdot p_{i,\omega,t}^{\mathrm{Ch}} \cdot (\frac{\Delta t}{3600})}{E_i^{ST}}) - (\frac{p_{i,\omega,t}^{\mathrm{DC}} \cdot (\frac{\Delta t}{3600})}{n_i^{ST} \cdot E_i^{ST}})) \tag{23}$$

$$\mathrm{SoC}_{i,(\min)}^{ST} \leq \mathrm{SoC}_{i,\omega,t} \leq \mathrm{SoC}_{i,(\max)}^{ST} \tag{24}$$

$$0 \leq p_{i,\omega,t}^{\mathrm{Ch}} \leq p_{i,\omega,t,(\max)}^{\mathrm{Ch}} \cdot u_{i,\omega,t}^{\mathrm{SoC}} \tag{25}$$

$$0 \leq p_{i,\omega,t}^{\mathrm{DC}} \leq n_i^{ST} \cdot p_{i,\omega,t,(\max)}^{\mathrm{DC}} \cdot (1 - u_{i,\omega,t}^{\mathrm{SoC}}) \tag{26}$$

$$q_{i(\min)}^{\mathrm{ESS}} \leq q_{i,\omega,t}^{\mathrm{ESS}} \leq q_{i(\max)}^{\mathrm{ESS}} \tag{27}$$

$$\mathrm{SoC}_{i,\omega,t_{\mathrm{end}}}^{ST} \geq \mathrm{SoC}_{\mathrm{thre}} \tag{28}$$

In the equations above, (23) calculates the SoC of ESSs. The limitation on the SoC of ESSs is set by (24). Constraints (25) and (26) guarantee that the active charged or discharged power by ESSs is within the limits considering their operation mode. Constraint (27) represents the reactive power limits of ESSs. Constraint (28) is to ensure that the SoC of ESSs is above a certain threshold $\mathrm{SoC}_{\mathrm{thre}}$ at the end of the simulation. n_i^{ST} is the conversion efficiency of the ESSs, E_i^{ST} represents the energy capacity, $p_{i,\omega,t}^{\mathrm{Ch}}$ and $p_{i,\omega,t}^{\mathrm{DC}}$ are respectively the charging and discharging active power of the ESS, and Δt is the duration of time intervals.

4) Power Balance Constraints: Each node should maintain a real and reactive power balance between the generated power and the demanded electricity.

$$\sum_{i=1}^{N_B} P_{i,\omega,t}^{\mathrm{fl}} = p_{i,\omega,t}^{\mathrm{MT}} + p_{i,\omega,t}^{\mathrm{WT}} + p_{i,\omega,t}^{s} + p_{\omega,t}^{\mathrm{UP}} + p_{i,\omega,t}^{\mathrm{Ch}} - p_{i,\omega,t}^{\mathrm{DC}} - p_{i,\omega,t}^{D} \tag{29}$$

$$\sum_{i=1}^{N_B} Q_{i,\omega,t}^{\mathrm{fl}} = q_{i,\omega,t}^{\mathrm{MT}} + q_{i,\omega,t}^{\mathrm{Ch}} - q_{i,\omega,t}^{D} \tag{30}$$

$$-M_1 * u_{ij,\omega,t}^{l} \leq P_{ij,t}^{\mathrm{fl}} \leq M_1 * u_{ij,\omega,t}^{l} \tag{31}$$

$$-M_1 * u_{ij,\omega,t}^{l} \leq Q_{ij,t}^{\mathrm{fl}} \leq M_1 * u_{ij,\omega,t}^{l} \tag{32}$$

Constraints (31) and (32) allow the power flow through each line only when $u_{ij,\omega,t}^{l}$ is equal to 1 meaning the line is online. The large-enough positive number M_1 is a relaxation parameter. The variables $p_{i,\omega,t}^{D}$ and $q_{i,\omega,t}^{D}$ are the supplied active and reactive power to the customers which are calculated by the load shedding $p_{i,\omega,t}^{\mathrm{shed}}$ subtracted from the original demand at each node $P_{i,\omega,t}^{\mathrm{demand}}$ in (33) and (34).

$$p_{i,\omega,t}^{D} = P_{\omega,t}^{\mathrm{demand}} - p_{\omega,t}^{\mathrm{shed}} \tag{33}$$

$$q_{\omega,t}^{D} = Q_{\omega,t}^{\mathrm{demand}} - q_{\omega,t}^{\mathrm{shed}} \tag{34}$$

$$0 \leq p_{i,\omega,t}^{\mathrm{shed}} \leq P_{i,\omega,t}^{\mathrm{demand}} \tag{35}$$

$$q_{i,\omega,t}^{\mathrm{shed}} = p_{i,\omega,t}^{\mathrm{shed}} \cdot \frac{Q_{i,\omega,t}^{\mathrm{demand}}}{P_{i,\omega,t}^{\mathrm{demand}}} \tag{36}$$

In (29), the active power $p_{\omega,t}^{\mathrm{UP}}$ represents the power exchange with the upstream system during the optimization. It depends on the energy purchases from or sold to the main grid and needs to be limited as shown in (37), (38), and (39). The binary variable $\varphi_{\omega,t}^{\mathrm{UP}}$ is used to determine buying (1) or selling (0) energy during the considered time horizon.

$$p_{\omega,t}^{\mathrm{UP}} = p_{\omega,t}^{\mathrm{UP_{buy}}} - p_{\omega,t}^{\mathrm{UP_{sell}}} \tag{37}$$

$$0 \leq p_{\omega,t}^{\mathrm{UP_{buy}}} \leq p_{\max}^{\mathrm{UP_{buy}}} \cdot \varphi_{\omega,t}^{\mathrm{UP}} \tag{38}$$

$$0 \leq p_{\omega,t}^{\mathrm{UP_{sell}}} \leq p_{\max}^{\mathrm{UP_{sell}}} \cdot (1 - \varphi_{\omega,t}^{\mathrm{UP}}) \tag{39}$$

B. Convexification and Linearization

The heat gain due to the ohmic losses presented in (7), is the multiplication of current flow square and conductor resistance. For an ohmic conductor, as shown in (9), the resistance can be calculated by a function of conductor temperature. In order to convexify the heat caused by the current, we consider that the resistance of the conductor is a constant value equal to its maximum at the highest temperature $T_{ij,(\max)}$. Also, the voltage is considered close to 1 p.u.. Applying this method, the current flow is equal to the apparent power flow and the equality constraint (7) is relaxed to the following inequality.

$$q_{ij,\omega,t}^{\mathrm{line}} \geq R^{\mathrm{line}}(T_{ij,(\max)} \cdot (|P_{ij,\omega,t}^{\mathrm{fl}}|^2 + |Q_{ij,\omega,t}^{\mathrm{fl}}|^2) \tag{40}$$

The radiation heat loss rate can be piece-wise linearized. The radiation heat loss depends on the fourth power of the conductor temperature as shown in (14). To piece-wise linearize this term, it is written as a function of the conductor temperature with a domain between the maximum conductor temperature and the ambient temperature. The radiation heat rate is finalized as in below:

$$q_{ij,\omega,t}^{\mathrm{rad}} = a \cdot T_{ij,\omega,t} + b \tag{41}$$

where a and b are the coefficients used in the radiated heat loss rate.

Based on the DistFlow branch equations in [22], constraint (42) and (43) represent the power flow equation. The large-enough positive number M_2 is a relaxation parameter to relax these two constraints for open branches. Constraint (44) states the boundary for the nodal voltage magnitudes across the power distribution network.

$$V_{\mathrm{sqr}_{i,t}} - V_{\mathrm{sqr}_{j,t}} \leq (1 - \alpha_{ij,t}) \cdot M_2 + 2 \cdot (r_{ij} \cdot P_{ij,t}^{\mathrm{fl}} + x_{ij} \cdot Q_{ij,t}^{\mathrm{fl}}), \quad \forall ij \in \mathbf{L}, \forall t \in \mathbf{T} \tag{42}$$

$$V_{\mathrm{sqr}_{i,t}} - V_{\mathrm{sqr}_{j,t}} \geq (\alpha_{ij,t} - 1) \cdot M_2 + 2 \cdot (r_{ij} \cdot P_{ij,t}^{\mathrm{fl}} + x_{ij} \cdot Q_{ij,t}^{\mathrm{fl}}), \quad \forall ij \in \mathbf{L}, \forall t \in \mathbf{T} \tag{43}$$

$$\underline{V_{\mathrm{sqr}_i}} \leq V_{\mathrm{sqr}_{i,t}} \leq \overline{V_{\mathrm{sqr}_i}}, \forall i \in \mathbf{B}, \forall t \in \mathbf{T} \tag{44}$$

IV. Case Study and Numerical Results

A. Test System Properties and Simulation Data

A modified IEEE 33-node test system [23] is considered to illustrate the effectiveness of the applied framework for resilient operation of the power distribution grids when facing wildfires. The single-line diagram of the considered test system is illustrated in Fig. 3. The test system is assumed

TABLE I
SIMULATION RESULTS FOR DIFFERENT NUMBER OF SCENARIOS

# of Scenarios	Objective Function ($\$\times 10^3$)	Load Shedding (MW)	Computation Time (s)
10	-52.31	2.52	21.5
50	-52.32	2.67	791.56
100	-52.95	2.96	3802.5

to be a balanced distribution grid with active peak demand equal to 11 MW. Since the distribution grid covers a small geographical area, its components all are subjected to similar environmental conditions. The location of ESSs, MTs, and RESs are depicted in Fig. 3 and the capacity of the distribution system components are taken from [8]. The cut-in, cut-out, and rated wind speeds for WTs are 4, 20, and 12 m/s, respectively. The PVs have a rated illumination intensity of 1000 $W/m2$. The weather parameters and wildfire information are derived from [7] and the wind and solar data are taken from [24], [25]. The standard deviation is calculated to be 15% of the mean value for wind speed and solar radiation and 5% of the mean value for loads. The von Mises distribution is supposed to have a k-factor of 2 [8]. The time step is considered 1 hour and the studied emergency horizon is 24 hours. The initial distance of the fire from the affected power lines are assumed as 1300 m and it is also assumed that the affected lines will be out of service until the end of the time horizon until which the fire will be suppressed. The SoC of the ESSs is expected to remain greater than 30% of the full potential, in order to contribute to demand fulfillment for the next hours after the analysis. An ASCR type of power line conductor is considered. The diameter and the maximum acceptable temperature of the power line is considered equal to 21 mm and 353 K°, respectively. All other data can be found in [8], [19]. The optimization problem is performed using CPLEX solver to handle the MILP optimization formulation. A General Algebraic Modeling System (GAMS) environment, using a PC with an Intel Xeon E5-2620 v2 processor, 16 GB of memory, and 64-bit operating system is used to solve and numerically analyze the results.

B. Resilient Operation of the Test System

The proposed framework in [8] is applied to this paper to enhance the distribution grid resilience when a progressive fire hits the grid. Different number of scenarios are considered to tackle the stochasticity of *wind speed*, *wind direction*, and *solar radiation*. For *Case I*, we assume that the fire only hits and affects the line 1-2. The simulation results reveal that line 1-2 will be out of order after $t = 19$ and the demand is not fully met. The numerical results for different number of scenarios are tabulated in Table. I. Since there is not a big difference between the objective function with different number of scenarios, the following analyses are presented with 10 number of scenarios. Note that in this paper, 10 number of scenarios satisfies the need of uncertainty consideration in wind speed, wind direction, and solar radiation. Figure 4 illustrates the expected energy exchange with the upstream

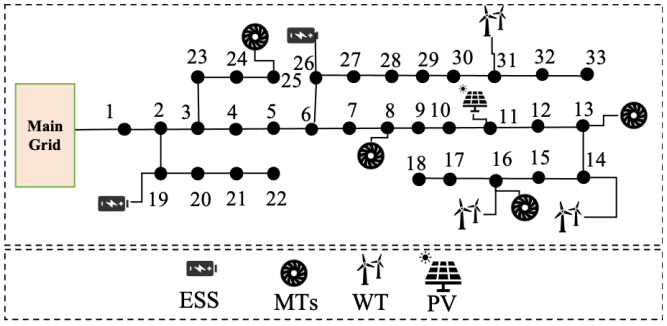

Fig. 3. Modified IEEE 33-node test system: The studied test system.

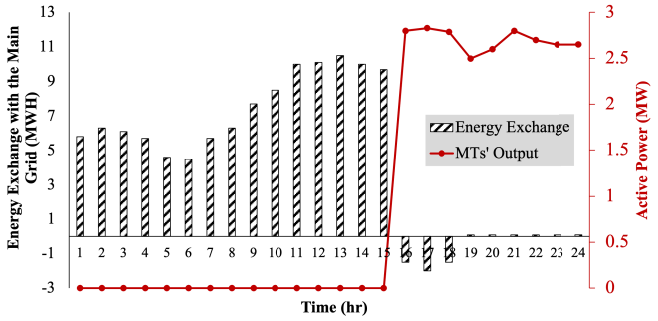

Fig. 4. Expected energy exchange with the main grid and the output generated power by MTs during the 24-hour time horizon.

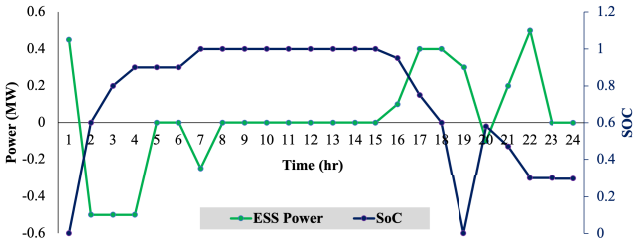

Fig. 5. Expected charging/discharging power and SoC of ESS at node 19.

network as well as the energy generated by MTs. One can see from the results that after $t = 16$, the energy is sold to the main grid since the cost of power generation by MTs is much lower than the purchasing energy from the main grid. Moreover, the expected energy exchanges drop significantly after $t = 18$ because of the unavailability of line 1-2. The expected discharging power and SoC of ESS at node 19 is depicted in Fig. 5.

C. Sensitivity Analyses

The applied framework is generic enough to be applied for the study of any distribution line approached by a progressive wildfire. In this section, two different lines are considered to be hit by the fire and we investigate how the system should proactively operate to ensure a resilient performance during the emergency. The expected energy exchange with the main grid for different cases are shown in Fig. 6 where *Case I* is the base case scenario when only line 1-2 is affected by wildfire, while *Case II*: line 1-2 and line 2-3; *Case III*: line 8-9 and

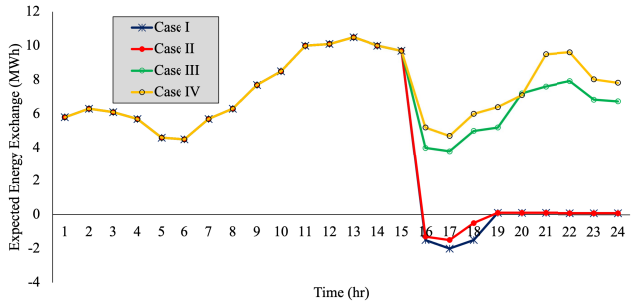

Fig. 6. Expected energy exchange for different cases.

line 9-10; and *Case IV*: line 3-23 and line 23-24 are assumed to be affected by the approaching wildfire. It is observed from Fig. 6, during the hours 15-24 when the wildfire hits the grid, those different combinations of affected lines by fire result in different expected energy exchange with the main grid. One can realize that the worst scenario is when the approaching fire hits line 1-2 and make the network isolated from the upstream network. For instance, the average of expected energy exchange with the main network after $t = 19$ for *Case II*, *Case III*, *Case IV* are respectively 0.0143, 6.6286, and 7.7714 MWh, while the expected energy exchange for *Case I* is 0. Hence, the role of ESSs, MTs, and RESs becomes much important in *Case I* compared to other cases. For instance, after the unavailability of line 1-2, MTs and ESSs supply respectively 18.69 and 1.3 MWh which highlights the importance and necessity of optimally employing local energy resources for resilience services during wildfire events.

V. Conclusion

This paper applied a general framework to enhance the power distribution system's operational resilience in the face of wildfire hazards. In particular, different aspects of wildfire are characterized first where DLR and the non-steady-state heat balance equations were used to mathematically model the impacts of wildfire on overhead power line conductor's temperature. The optimization model aimed to minimize the load outages and the corresponding consequences in the grid during wildfires. Different scenarios were fed into the mixed-integer linear optimization formulation to overcome the prevailing uncertainties of RESs distributed across the power distribution network. The numerical results revealed that the load outage could be remarkably reduced if the progressive wildfire is characterized in advance and all local resources, i.e., RESs, MTs, and ESSs, are strategically and optimally coordinated.

References

[1] S. E. DeYoung, J. Chase, M. P. Branco, and B. Park, "The effect of mass evacuation on infant feeding: the case of the 2016 fort mcmurray wildfire," *Maternal and child health journal*, vol. 22, no. 12, pp. 1826–1833, 2018.

[2] D. Jones. October wildfire claims top 9.4 billion statewide,2017, [Online] Available:http://www.insurance.ca.gov/0400-news/0100-press-releases/2017/release135-17.cfm.

[3] Times Editorial Board, Wildfires are natural disasters but Congress refuses to budget for them, Los Angeles Times, Jan. 2018, [Online] Available: https://www.latimes.com/opinion/editorials/la-ed-wildfire-funding-fix-20180102-story.html.

[4] US Forest Service Report, "The Rising Cost of Fire Operations: Effects on the Forest Service's Non-Fire Work", US Department of Agriculture, Aug. 2015.

[5] Top 10 Costliest Wildland Fires in The United States, [Online] Available: https://www.iii.org/table-archive/21424.

[6] [Online] Available: https://www.utilitydive.com/news/the-hard-choice-californias-wildfires-have-forced-on-its-utilities-and-a/548614/.

[7] M. Choobineh, B. Ansari, and S. Mohagheghi, "Vulnerability assessment of the power grid against progressing wildfires," *Fire Safety Journal*, vol. 73, pp. 20–28, 2015.

[8] D. N. Trakas and N. D. Hatziargyriou, "Optimal distribution system operation for enhancing resilience against wildfires," *IEEE Transactions on Power Systems*, vol. 33, no. 2, pp. 2260–2271, 2017.

[9] A. Bagchi, A. Sprintson, and C. Singh, "Modeling the impact of fire spread on an electrical distribution network," *Electric Power Systems Research*, vol. 100, pp. 15–24, 2013.

[10] S. Mohagheghi and S. Rebennack, "Optimal resilient power grid operation during the course of a progressing wildfire," *International Journal of Electrical Power & Energy Systems*, vol. 73, pp. 843–852, 2015.

[11] B. Ansari and S. Mohagheghi, "Optimal energy dispatch of the power distribution network during the course of a progressing wildfire," *International Transactions on Electrical Energy Systems*, vol. 25, no. 12, pp. 3422–3438, 2015.

[12] J. W. Mitchell, "Power line failures and catastrophic wildfires under extreme weather conditions," *Engineering Failure Analysis*, vol. 35, pp. 726–735, 2013.

[13] D. Coldham, A. Czerwinski, and T. Marxsen, "Probability of bushfire ignition from electric arc faults," *HRL Technology Pty Ltd., Melbourne, VIC., Australia, Tech. Rep. HRL/2010/195*, 2011.

[14] E. I. Koufakis, P. T. Tsarabaris, J. S. Katsanis, C. G. Karagiannopoulos, and P. D. Bourkas, "A wildfire model for the estimation of the temperature rise of an overhead line conductor," *IEEE transactions on power delivery*, vol. 25, no. 2, pp. 1077–1082, 2010.

[15] S. Jazebi, F. De Leon, and A. Nelson, "Review of wildfire management techniques-part i: Causes, prevention, detection, suppression, and data analytics," *IEEE Transactions on Power Delivery*, 2019.

[16] J.-L. Rossi, A. Simeoni, B. Moretti, and V. Leroy-Cancellieri, "An analytical model based on radiative heating for the determination of safety distances for wildland fires," *Fire Safety Journal*, vol. 46, no. 8, pp. 520–527, 2011.

[17] I. Z. F. bin Hussien, A. A. Rahim, and N. Abdullah, "Electric power transmission," in *Alternative Energy in Power Electronics*, pp. 317–347, Elsevier, 2011.

[18] "Ieee standard for calculating the current-temperature relationship of bare overhead conductors," *IEEE Std 738-2012 (Revision of IEEE Std 738-2006 - Incorporates IEEE Std 738-2012 Cor 1-2013)*, pp. 1–72, 2013.

[19] F. Teng, "Enhancing power distribution grid resilience against massive wildfires," Master's thesis, The George Washington University, 2020.

[20] M. Panteli, D. N. Trakas, P. Mancarella, and N. D. Hatziargyriou, "Boosting the power grid resilience to extreme weather events using defensive islanding," *IEEE Transactions on Smart Grid*, vol. 7, no. 6, pp. 2913–2922, 2016.

[21] Z. Liu, F. Wen, and G. Ledwich, "Optimal siting and sizing of distributed generators in distribution systems considering uncertainties," *IEEE Transactions on power delivery*, vol. 26, no. 4, pp. 2541–2551, 2011.

[22] M. E. Baran and F. F. Wu, "Network reconfiguration in distribution systems for loss reduction and load balancing," *IEEE Transactions on Power delivery*, vol. 4, no. 2, pp. 1401–1407, 1989.

[23] C. Wang and H. Z. Cheng, "Optimization of network configuration in large distribution systems using plant growth simulation algorithm," *IEEE Transactions on Power Systems*, vol. 23, no. 1, pp. 119–126, 2008.

[24] D. Papaioannou, C. Papadimitriou, A. Dimeas, E. Zountouridou, G. Kiokes, and N. Hatziargyriou, "Optimization & sensitivity analysis of microgrids using homer software-a case study," 2014.

[25] PVWattsCalculator, [Online] Available:http://pvwatts.nrel.gov.